Pergamon

Int. J. Heat Mass Transfer. Vol. 39, No. 11, pp. 2283–2292, 1996

0017-9310/96 $15.00 + 0.00

0017-9310(95)00287-1

Bulk flow pulsations and film cooling—II. Flow structure and film effectiveness

P. M. LIGRANI, R. GONG and J. M. CUTHRELL

Convective Heat Transfer Laboratory, Department of Mechanical Engineering, University of Utah, Salt Lake City, UT 84112, U.S.A.

and

J. S. LEE

Turbo and Power Machinery Research Center, Department of Mechanical Engineering, Seoul National University, Seoul 151-742, Korea

(*Received for publication* 14 *August* 1995)

Abstract—Experimental results are presented which describe the effects of bulk flow pulsations on film cooling from a single row of simple angle film cooling holes. The pulsations are in the form of sinusoidal variations of static pressure and streamwise velocity. Distributions of time-averaged Reynolds shear stress are presented for quasi-steady film conditions at x/d of 4.5, 9.8, 16.4 and 24.1, where x is streamwise distance from the downstream edge of the holes and d is hole diameter. Distributions of streamwise mean velocity are also presented for the same locations. Important changes from the imposed bulk flow pulsations are evident in all measured quantities, especially just downstream of the holes at $x/d = 4.5$. Important changes to local and spanwise-averaged film effectiveness also occur as the coolant Strouhal number becomes greater than 1–2 and the film moves from quasi-steady to non-quasi-steady behavior. Copyright © 1996 Elsevier Science Ltd.

INTRODUCTION

The present paper is a companion to Ligrani *et al.* [1] in which the changes to injectant resulting from the imposition of bulk flow pulsations in the form of periodic variations of *static* pressure and streamwise velocity are described. Here, the effects of bulk flow pulsations are discussed as they affect the structure and film effectiveness of film cooled boundary layers. Structure is described in terms of distributions of streamwise mean velocity and the Reynolds shear stress. These are measured at four different streamwise stations downstream of the holes ($x/d = 4.5$, 9.8, 16.4 and 24.1) at $z/d = 0$, and across the test surface span at $x/d = 4.5$. Local magnitudes of film effectiveness are also given for the same x/d. These results are important because they further substantiate the effects of the imposed pulsations on boundary layer film cooling. As such, additional insight is provided into the influences of potential flow interactions and passing shock waves on film cooled boundary layers developing on turbine surfaces.

EXPERIMENTAL APPARATUS AND PROCEDURES

The experiment is conducted using the same wind tunnel, film cooling configuration, injectant air supply, and pulsation generation techniques employed by Ligrani *et al.* [1]. A schematic of the wind tunnel test section including the coordinate system is shown in Fig. 1.

Flow conditions

The turbulence structure surveys presented here are measured at $\overline{u_\infty} = 10$ m s^{-1}. At $x/d = 4.5$, this gives $\delta/d = 1.15$, a ratio of displacement thickness to hole diameter of 0.178, and a ratio of momentum thickness to hole diameter of 0.127. For x/d from 4.5 to 24.1, Reynolds numbers based on streamwise distance (from the trip) then range from 740 000 to 1 016 000. With the pulsations, the film cooling is quasi-steady [1] with coolant Strouhal number St_c equal to 0.11 and freestream Strouhal number St_∞ equal to 0.031. Blowing ratio $\overline{m}$ is 0.98, momentum flux ratio is 0.96, and ratio of injectant to freestream density ρ_c/ρ_∞ is 1.0. Injection hole diameter is 2.22 cm, and injection Reynolds number $d\overline{u_c}/\nu$ is then about 15 000. The test conditions for the turbulence structure surveys are different from the ones in ref. [1] because they were chosen to provide quasi-steady film behavior at flow conditions where accurate hot-wire anemometry measurements can be made.

The film effectiveness results are measured at the same conditions as the injectant surveys presented in ref. [1]. For these tests, freestream velocity $\overline{u_\infty}$ is 2.0 m s^{-1}, blowing ratio $\overline{m}$ is 0.25, and the ratio of injectant to freestream density ρ_c/ρ_∞ is about 0.9.

Mean velocity and turbulence structural details

Boundary layer mean velocity components and Reynolds stress tensor components are measured

NOMENCLATURE

d	injection hole diameter
l	injection hole length
$\overline{m}$	blowing ratio, $\rho_c\overline{u_c}/\rho_\infty\overline{u_\infty}$
n	pulsation frequency [Hz]
St_c	coolant Strouhal number, $2\pi nl/\overline{u_c}$
St_∞	freestream Strouhal number, $2\pi n\delta/\overline{u_\infty}$
t	temperature, time
u	streamwise velocity
$\overline{u_c}$	time-averaged injectant velocity, spatially averaged over hole cross-section
$\overline{u_\tau}$	friction velocity
v	normal velocity
w	spanwise velocity
x	streamwise distance measured from downstream edge of injection holes
X	streamwise distance measured from trip
y	distance normal to the surface
y^+	$y\overline{u_\tau}/v$
z	spanwise distance from test surface centerline.

Greek symbols

δ	boundary layer thickness
η	local film cooling effectiveness based on injectant temperature averaged over exit planes of injection holes $(t_{aw}-t_{r\infty})/(t_{rc}-t_{r\infty})$
η_c	local η at $z/d=0$
ρ	density
τ	time period of one pulsation
ν	kinematic viscosity.

Subscripts

aw	adiabatic wall
c	injectant at exit plane of injection holes
cc	injectant hole centerline value at exit plane of injection holes
0	stagnation condition
r	recovery condition
∞	freestream.

Superscripts

$'$	fluctuating component
$\overline{\ }$	time average
$\sim$	periodic component
$\wedge$	phase average.

using hot-wire anemometry probes. A Dantec 55P05 hot-wire probe, with gold plated leads, sensor diameter of 5 μm and sensor length of 1.25 mm, is used to measure the instantaneous longitudinal velocity u. A Dantec 55P51 crossed-hot wire probe, also with gold plated leads and sensors having the same approximate diameter and sensor length, is used to measure u and v simultaneously. Disa 55M10 constant-temperature bridges are used to operate all of the sensors at an overheat ratio of 1.6. The hot-wire is calibrated in the potential flow of the wind tunnel with the same bridge settings employed for measurements. Hot-wire velocity calibrations are conducted with the crossed-wire probe oriented both in the uv plane and the uw plane, and yaw calibrations are conducted with the probe in the uw plane to determine the effective wire angles with respect to the streamwise flow direction. Calibrations are repeated at each new streamwise measurement location and for each new survey, because effective wire angles change slightly as the probe sensors are rotated and as the probe traversing mechanism is relocated. During calibrations and measurements, the voltage signal from each hot-wire bridge is processed using a Dantec Model 56N20 signal conditioner system set with an amplifier gain of 1, a low-pass filter of 3 kHz, and no high pass filter.

Data acquisition system

Signals from the signal conditioners connected to the hot-wire anemometry bridges are acquired using a Hewlett-Packard 3852A data acquisition control unit. This unit operates with a Hewlett-Packard 44702A high speed voltmeter, Hewlett-Packard 44711A high-speed FET multiplexers, and Hewlett-Packard 44703B extended memory cards. The control unit with installed components is controlled and programed using a Hewlett-Packard model A2240B type 362 mainframe computer. The system is capable of acquiring up to 24 channels of data at a total rate up to 100 kHz (for all channels).

Local adiabatic film cooling effectiveness

Local magnitudes of the adiabatic film cooling effectiveness along the test surface are determined from near wall measurements of temperature as the injectant is heated to approximately 50°C and no heat is applied to the test surface. For the distributions, a copper–constantan thermocouple is traversed just above the test surface using an automated computer-controlled two-dimensional traversing system which

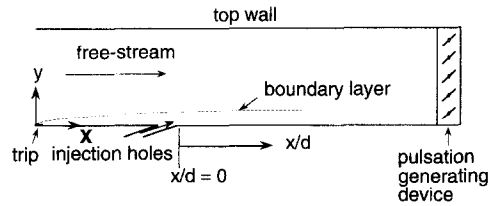

Fig. 1. Schematic of test section and coordinate system.

may be placed at different streamwise locations. With this traverse, the thermocouple probe is traversed over 40 locations spaced 0.51 cm apart across the span of the wind tunnel test section. As the boundary layer is probed at each measurement location, simultaneous measurements are made of the injectant temperature (at hole exits), and freestream temperature. Voltages from thermocouples are digitally sampled and read using Hewlett-Packard 44422 relay multiplexer cards for type T thermocouples, and a Hewlett-Packard 3497A Data Acquisition Control Unit with a 3498A Extender. These units are controlled and resulting data are processed using the Hewlett-Packard model A2240B type 362 mainframe computer.

PHASE-AVERAGE AND DATA PROCESSING

Instantaneous voltages are converted into instantaneous velocities using look-up tables which minimize the times required to compute the turbulence statistical quantities. For each measurement location, a total of 14 000 data points are acquired for each of two channels at a rate of 4 kHz per channel, giving a total sampling time of 3.5 s. Each spanwise/normal plane survey covers a grid of 15 by 12 locations spaced 0.508 cm apart. Because total survey time is 19.2 h (actually conducted in two parts), freestream air temperature is not constant, and calibration coefficients are corrected for air temperature variations as the survey is conducted using procedures described by Perry [2].

With imposed periodic flow, instantaneous velocities u can be considered to be the sum of three components such that $u = \bar{u}+\tilde{u}+u'$, where $\bar{u}$ is the time-averaged velocity, $\tilde{u}$ is the periodic velocity and u' is the fluctuating component [3]. In the present study, $\bar{u}$ and $\tilde{u}$ are combined as the phase-averaged velocity $\hat{u}$, such that $u = \hat{u}+u'$ [4]. Thus, for a steady flow with no periodic velocity, $\hat{u}$ is then equal to $\bar{u}$. $\hat{u}$ is then determined from phase-averaging instantaneous velocity results using the equation given by

$$\hat{u}(n)\,|_{n=1}^{2000} = \frac{1}{npulse}\sum_{m=1}^{npulse} u(m,n)|_{n=1}^{2000}$$

where m and n correspond to the number of pulsations and to the number of locations across each phase where data are sampled, respectively, and *npulse* denotes total number of pulsations.

Phase-averaging is accomplished here using procedures developed exclusively for this study. After the velocities u, or u and v are determined at a particular probe location, $\bar{u}$, the time-averaged magnitude of the longitudinal velocity is calculated. The overall average pulsation time period and overall average frequency of the pulsations are then determined. After this is accomplished, all velocity samples are adjusted to account for the fact that the overall pulsation period does not coincide exactly with an exact integer multiple of the time period between data samples. Phase-averaged velocities ($\hat{u}$), and time-averaged Reynolds shear stress magnitudes ($-\overline{u'v'}$) are then determined.

For the present study, the pulsating generating device produces near-sinusoidal velocity (and static pressure) wave forms at a frequency of 2 Hz at peak-to-peak amplitudes from 40% of $\bar{u}$ in the freestream of 125% of $\bar{u}$ near the wall. The pulsations propagate throughout the wind tunnel test section, including all locations within the boundary layer developing along the test surface. The sinusoidal form for the wave form is easily described and deterministic allowing the effects of different parts of the wave form (i.e. high and low static pressures, high and low velocities, accelerations and decelerations) on film cooling to be clearly discerned.

An example of instantaneous velocity data is shown in the top of Fig. 2, along with the corresponding traces of phase-averaged velocity $\hat{u}$ and phase-averaged fluctuating velocity $\widehat{u'^2}$. At the bottom of the figure, a trace of $\bar{u}+u'$ is shown determined from $u-\tilde{u}$. These data illustrate the sinusoidal nature of the

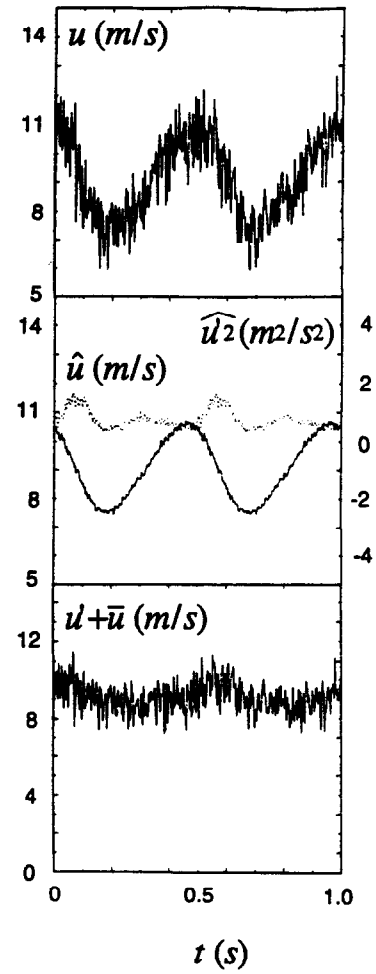

Fig. 2. Instantaneous phase-averaged, and fluctuating streamwise velocity in a turbulent boundary layer with pulsations imposed at 2 Hz at $X = 0.191$ m, $z = 0.0$ m, $y/\delta = 0.46$, $y^+ = 154$ and $St_x = 0.016$.

velocity wave form produced by the pulsation device. Another interesting feature is the destabilizing effect of decelerations and the stabilizing influence of accelerations, evident from respective increases and decreases of $u' + \bar{u}$ and $\widehat{u'^2}$. The data presented in Fig. 2 were obtained from a sample of 14000 data points acquired at 400 Hz per channel at $X = 0.191$ m, $z = 0.0$ m, $y/\delta = 0.46$, and y^+ of 154 in a boundary layer with pulsations imposed at 2 Hz ($St_\infty = 0.016$) and no film cooling.

BASELINE TEST RESULTS

A number of baseline tests were conducted, including: (a) no film cooling and no pulsations, and (b) with bulk flow pulsations and no film cooling. With no pulsations and no film cooling, normalized profiles of $\overline{u^2}$, $\overline{v^2}$, $\overline{w^2}$, and $-\overline{u'v'}$ show behavior characteristics of turbulent boundary layers with two-dimensional mean flow fields, and excellent agreement with the measurements of Green [5] and Klebanoff [6], after accounting for a different freestream turbulence level in the latter case.

Profiles of $\sqrt{\overline{u'^2}}/\overline{u_\infty}$ and $\sqrt{\overline{v'^2}}/\overline{u_\infty}$ obtained in turbulent boundary layers, both with and without pulsations and no film cooling, are compared to measurements from Menendez and Ramaprian [7] in Fig. 3. The present results with pulsations at 2 Hz are presented for $X = 0.813$ m, $z = 0.0$ m, $\delta = 2.63$ cm, $\overline{u_\infty} = 10$ m s^{-1}, $\overline{u_\tau} = 0.447$ m s^{-1}, and $St_\infty = 0.033$, and are in agreement with the ones from Menendez and Ramaprian [7], considering slightly different experimental conditions in the two studies. The most important common features are the slight decreases of $\sqrt{\overline{u'^2}}/\overline{u_\infty}$ and $\sqrt{\overline{v'^2}}/\overline{u_\infty}$ which occur due to the imposed pulsations. In both investigations, these decreases occur relative to the profiles obtained with no pulsations over significant portions of the boundary layers.

The agreement of these baseline measurements with ones from other sources validates the experimental apparatus and procedures, and provides confidence that the results obtained with film cooling and pulsations are accurate.

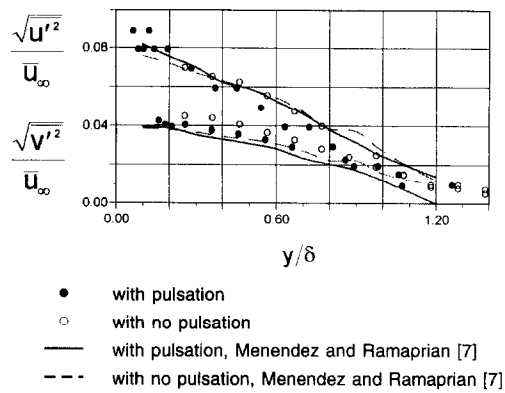

Fig. 3. Profiles of normalized normal Reynolds stress components obtained with and without pulsations at 2 Hz in a turbulent boundary layer at $X = 0.813$ m, $z = 0.0$ m, $\delta = 2.63$ cm, $\overline{u_\infty} = 10$ m s^{-1}, $\overline{u_\tau} = 0.447$ m s^{-1} and $St_\infty = 0.033$.

EXPERIMENTAL RESULTS—STREAMWISE MEAN VELOCITY

Profiles of $\bar{u}/\overline{u_\infty}$ measured at $x/d = 4.5$ and z/d of 0.00, 0.23, 0.46, 0.69, 0.91 and 1.14 are now discussed in reference to Fig. 4. Profiles of $\bar{u}/\overline{u_\infty}$ measured at $z/d = 0$ and x/d of 4.5, 9.8, 16.4 and 24.1 are then presented in Fig. 5. At each location, profiles are presented for three situations: (i) no film, no pulsations; (ii) with film, no pulsations; and (iii) with film and with pulsations.

Flow structure with no pulsations, variations with z/d

Considering results with no pulsations, the streamwise mean velocity distributions in Fig. 4 show three different regions of behavior across the span of the measurement plane. The first region exists at z/d from 0.0 to 0.46, the second region is present at z/d from 0.69 to 0.91 and the third region is evident at $z/d = 1.14$.

The *first region* corresponds to locations containing the highest film concentrations. Just downstream of the holes, this region extends from the wall to y/d of approximately 1.5 and from $z/d = -0.60$ to $z/d = 0.60$. It is characterized by positive magnitudes of normal velocity $\bar{v}$ from 0.00 $\overline{u_\infty}$ to 0.18 $\overline{u_\infty}$ resulting from the upward trajectory of the film as it moves away from the holes [8]. Figure 4 shows that streamwise velocities in this first region are characterized by a large gradient (with respect to y/d) at y/d from 1.0 to 1.5 which corresponds to the outer portion of the film concentration. The gradient evidences a shear layer developing at the interface between fluid with low streamwise momentum (below) and fluid with high streamwise momentum (above). As y/d becomes greater than 1.0–1.5, streamwise velocities in the boundary layer with film cooling and no pulsations then increase, and normal velocities approach zero. At $y/d > 2.0$–2.5, $\bar{u}/\overline{u_\infty}$ in Fig. 4 then approach the profile with no film cooling.

Below the $\bar{u}/\overline{u_\infty}$ gradient at $y/d < 1.0$–1.5, streamwise velocities from film cooling are generally less than ones present with no film cooling (again only considering data with no pulsations). These are a result of low streamwise momentum fluid which is entrained by the film and then advected away from the wall by the positive $\bar{v}$ velocities. As y/d becomes less than 0.5–0.7 at $z/d = 0.23$ and 0.46, $\bar{u}/\overline{u_\infty}$ with film cooling and no pulsations are higher than ones present with no film cooling and no pulsations.

The shear layer which characterizes the first region is no longer present in the *second region* located at $z/d = 0.69$ and 0.91. Here, profiles of $\bar{u}/\overline{u_\infty}$ in Fig. 4 show values which are significantly greater than ones measured with no film cooling, especially for

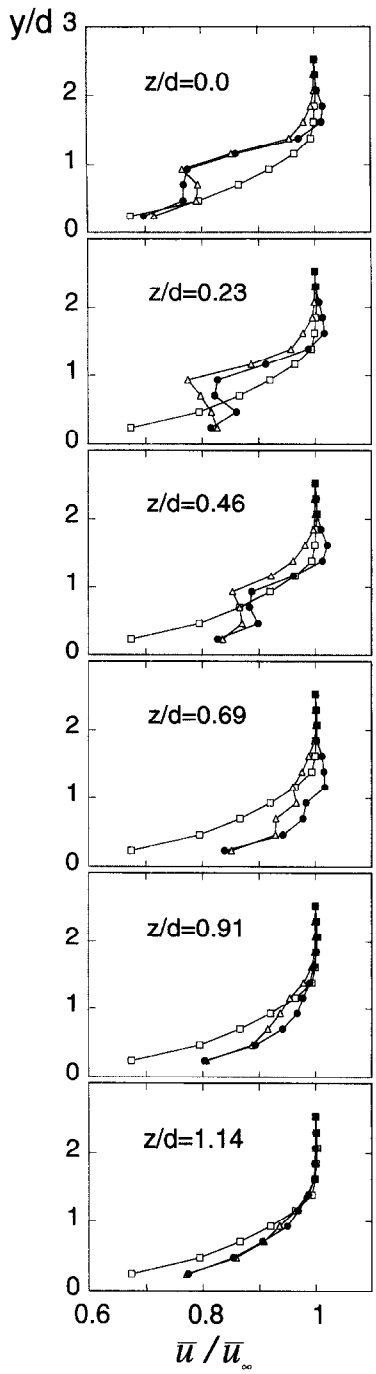

Fig. 4. Spanwise variation of profiles of normalized time-averaged streamwise velocity $\bar{u}$ at $x/d = 4.5$ with quasi-steady film behavior. Symbol labels are given with Fig. 5.

$y/d < 1.0$–1.5. This is partially a result of the downwash portions of the legs of the horseshoe vortex which forms just upstream of each injection hole around the most important injectant concentrations. The vortex acts to advect high momentum fluid from the freestream, boundary layer, and injectant towards the wall at $z/d = 0.69$ and 0.91. Here, $\bar{v}$ are negative, and $\bar{v}/u_\infty$ range from 0.0 to -0.09 indicating significant normal velocities towards the wall [8].

The *third region* at $z/d = 1.14$ in Fig. 4 is characterized by a film cooled $\bar{u}/\overline{u_\infty}$ profile (obtained with no pulsations) which approaches the profile with no film and no pulsations.

Flow structure with no pulsations, variations with x/d

Figure 5 shows the streamwise development of $\bar{u}/u_\infty$ profiles measured at $z/d = 0$. Considering results with no pulsations, streamwise velocities for the boundary layer with film cooling are generally less than ones measured with no film cooling at all four x/d. This is a result of low streamwise momentum fluid which is entrained by the film and then advected away from the wall by the positive magnitudes of normal velocity $\bar{v}$, as mentioned earlier. As the boundary layer advects downstream to larger x/d, Fig. 5 shows film cooled profiles of $\bar{u}/\overline{u_\infty}$ with qualitative characteristics similar to the $x/d = 4.5$ profile. The most important quantitative differences pertain to the location and intensity of the shear layer, which is located farther from the wall with normal gradient $\bar{u}/\overline{u_\infty}$ magnitudes that decrease as x/d increases.

Effects of pulsations on flow structure, variations with z/d

Significant changes to the flow structure occur when the pulsations are present. Figure 4 shows that the most important change in the film cooled boundary layer at z/d of 0.23, 0.46, 0.69 and 0.91 is higher $\bar{u}/\overline{u_\infty}$ with pulsations over most of the boundary layer thickness. Different behavior occurs at $z/d = 0.0$, where values with pulsations are lower than ones with no pulsations for $y/d = 0.4$–0.9, about the same for $y/d = 0.9$–1.35, and higher than the ones with no pulsations at y/d from 1.35–2.0. Thus, the same $\bar{u}/\overline{u_\infty}$ gradient is present in the film cooled boundary layer both with and without pulsations, but it extends over a larger vertical portion of the boundary layer at $z/d = 0.0$ when the pulsations are imposed. As this occurs in the outer portion of the boundary layer, the effect is so dramatic that streamwise velocities are locally higher than the freestream velocity at $z/d = 0.0$, 0.23, 0.46 and 0.69.

Effects of pulsations on flow structure, variations with x/d

Figure 5 shows $\bar{u}/\overline{u_\infty}$ from the pulsating boundary layer which are lower than the values measured with no pulsations for $y/d < 0.9$–1.5 at x/d of 4.5, 9.8 and 16.4. At larger y/d, the pulsating film cooled profiles are the same as the ones measured in the boundary layers with no pulsations, with the exception of the results at $x/d = 0$. Thus, the same $\bar{u}/\overline{u_\infty}$ shear layer gradient extends over a larger vertical portion of the boundary layer at x/d of 4.5, 9.8 and 16.4 when the pulsations are imposed. As x/d reaches 24.1 in Fig. 5, the film cooled profile measured with pulsations

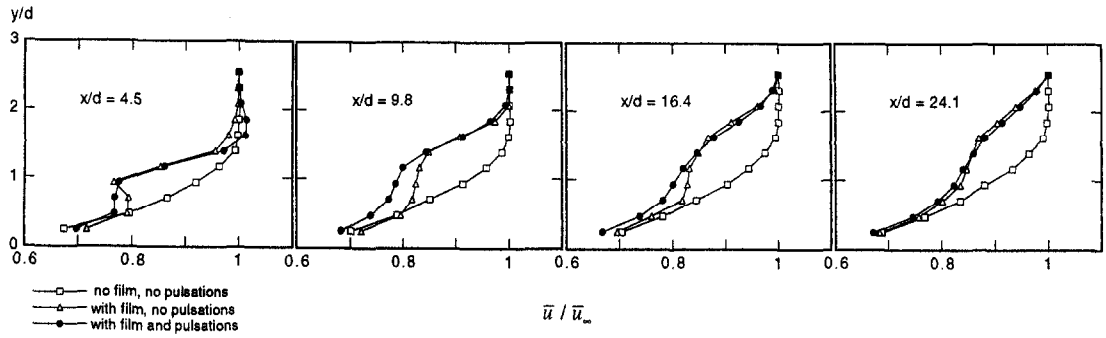

Fig. 5. Streamwise development of profiles of normalized time-averaged streamwise velocity $\bar{u}$ at $z/d = 0$ with quasi-steady film behavior.

approaches the film cooled profile measured with no pulsations.

Overall effects of the pulsations

The structural characteristics resulting from the pulsations are present because the imposed pulsations produce periodically unsteady static pressure fields at the exits of the injection holes, which result in pulsating coolant flow rates [1]. In addition, the pulsating static pressure and velocity fields in the boundary layer just downstream from the injection holes result in complex variations with time of the trajectories, distributions, as well as the coverage of the injectant along the surface [1]. The film thus instantaneously changes its momentum and position in the boundary layer when bulk flow pulsations are imposed. The mean injectant trajectory with pulsations is also somewhat different, and the same amount of injectant is spread over a larger volume compared to non-pulsating flow.

The local streamwise velocities which are higher than the freestream velocity ($\bar{u}/\overline{u_\infty} > 1$) at $x/d = 4.5$ in Figs. 4 and 5 are then due to the behavior of the injectant when its momentum is highest during each pulsation cycle. During each of these intervals, instantaneous m reach 1.07, which give local injectant velocities as large as about $1.10\overline{u_\infty}$ at the injection hole exits. $\bar{u}/\overline{u_\infty}$ is then greater than 1 just downstream of the hole exits, and the injectant is lifted farther away from the wall than the trajectory produced with no pulsations when $\overline{m}$ is constant at 0.98. Streamwise velocities are then locally higher than the freestream at $z/d = 0.0$–0.69 and at x/d as large as 4.5.

As the static pressure at the hole exits increases, u_c decreases to 9.64 m s^{-1} which gives $u_c/\overline{u_\infty} = 0.89$ and the lowest injectant momentum at the injection hole exits during each pulsation cycle. The injectant is then located closer to the wall than the trajectory produced when no pulsations are imposed. As a result, streamwise velocities are locally lower than the velocities measured at the same y/d when no pulsations are imposed. This is evident for $y/d < 0.9$ and $x/d = 4.5$ and $z/d = 0.0$ in Fig. 4, and for $y/d < 0.9$–1.5 in Fig. 5 for $x/d = 4.5$, 9.8 and 16.4.

EXPERIMENTAL RESULTS—REYNOLDS SHEAR STRESS

Profiles of $-2\overline{u'v'}/\overline{u_\infty^2}$ in film cooled boundary layers both with and without pulsations are presented in Figs. 6 and 7, respectively, along with baseline profiles with no pulsations and no film cooling. The results in Fig. 6 are presented for $x/d = 4.5$ at $z/d = 0.0$, 0.23, 0.46, 0.69, 0.91 and 1.14, and the data in Fig. 7 are given at $z/d = 0$ for $x/d = 4.5$, 9.8, 16.4 and 24.1. The experimental conditions are the same as for the Figs 4 and 5 results.

Flow structure with no pulsations, variations with z/d

The film cooled $-2\overline{u'v'}/\overline{u_\infty^2}$ distributions in Fig. 6 (with no pulsations) are significantly different from the ones with no film cooling (and no pulsations). As for the $\bar{u}/\overline{u_\infty}$ results, three different regions are apparent, each containing a qualitatively different type of flow behavior, as one moves across the span of the measurement plane.

For the *first* region at z/d of 0.00, 0.23 and 0.46, each profile in Fig. 6 shows an important local maxima in $-2\overline{u'v'}/\overline{u_\infty^2}$ located about $1.0d$ from the wall. Here, magnitudes of maximum $-2\overline{u'v'}/\overline{u_\infty^2}$ are much higher than measured at the same location with no film and no pulsations because of high production of turbulence ($-\overline{u'v'}(\partial\bar{u}/\partial y)$). The shear layer (mentioned earlier) at the interface between fluid with low streamwise momentum below and fluid with much higher streamwise momentum above is responsible. This region of high $-2\overline{u'v'}/\overline{u_\infty^2}$ is bounded by regions above and below where the normalized Reynolds shear stress is sometimes negative and significantly lower than measured in the baseline boundary layer. This behavior is due to the advection of fluid with low streamwise momentum away from the wall, as well as the streamwise advection of the film from the holes.

The *second* region of qualitative behavior across the span of the measurement plane, located at $z/d = 0.69$ and 0.91, is characterized by magnitudes of $-2\overline{u'v'}/\overline{u_\infty^2}$ in Fig. 6 which are less than ones measured with no pulsations and no film cooling over the entire boundary layer thickness. In addition $-2\overline{u'v'}/\overline{u_\infty^2}$

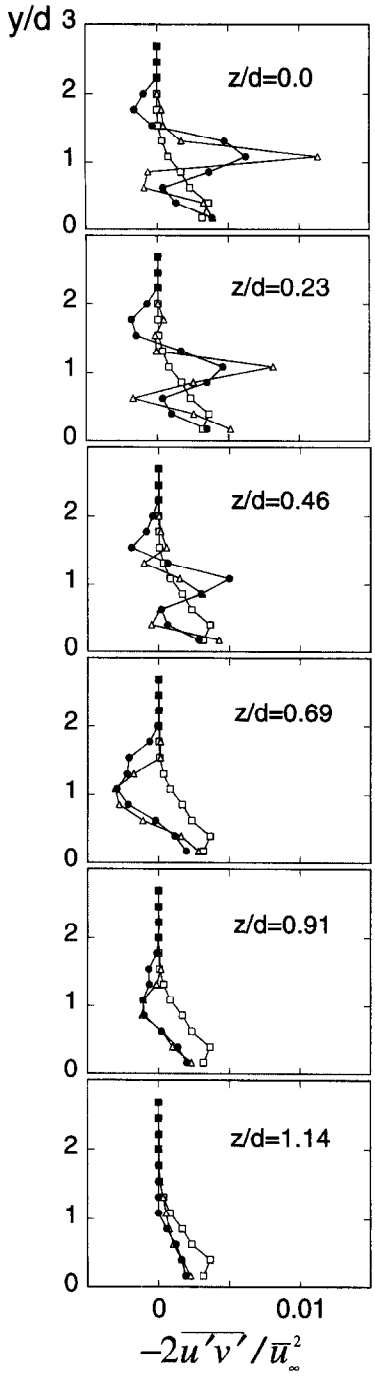

Fig. 6. Spanwise variation of profiles of normalized $-2\overline{u'v'}$ Reynolds shear stress at $x/d = 4.5$ with quasi-steady film behavior. Symbol labels are given with Fig. 7.

values are negative at $y/d > 0.5$–0.7. As mentioned earlier, the presence of the film brings much fluid with high streamwise momentum close to the wall in this part of the flow. As a result, steamwise mean velocities are higher than ones in the baseline boundary layer over much of the boundary layer thickness, and the normal component of mean velocity $\bar{v}$ is negative. The result is a turbulent boundary layer which is highly three-dimensional.

The *third* region of qualitative behavior is evident at $z/d = 1.14$. The film cooled $-2\overline{u'v'}/\overline{u}_\infty^2$ profile in Fig. 6 (obtained with no pulsations) at this spanwise location is positive over the entire boundary layer thickness. Compared to the other profiles at smaller z/d, it is quite similar to the profile with no pulsations and no film. The influences of the film cooling are minimal at this spanwise location, and mean velocity components in Figs. 4 and 5 are approaching behavior characteristic of turbulent boundary layers with two-dimensional mean flow fields.

Flow structure with no pulsations, variations with x/d

As x/d increases to 9.8–24.1, Fig. 7 shows that the intensity of the shear layer decreases and that magnitudes of $-2\overline{u'v'}/\overline{u}_\infty^2$ decrease. Local maxima are located farther from the wall, regions of negative $-\overline{u'v'}$ are no longer present, and $-2\overline{u'v'}/\overline{u}_\infty^2$ gradients are much smaller than measured at $x/d = 4.5$. The outer portions of the film cooled boundary layers at $x/d = 9.8$–24.1 are then characterized by $-2\overline{u'v'}/\overline{u}_\infty^2$ which are greater than in the baseline boundary layer with no film cooling. The inner portions are characterized by $-2\overline{u'v'}/\overline{u}_\infty^2$ which are then lower than baseline boundary layer magnitudes. The y/d boundary between these two regions increases with streamwise development, ranging from 1.0 to 1.4.

Effects of pulsations on flow structure, variations with z/d

As for the mean velocity components, significant changes to the Reynolds shear stresses occur when the pulsations are present. One of the most important effects is alteration of the positions of different flow structures with time. In particular, the most important film concentrations move to and from the wall with each flow oscillation and probably change shape and extent in the spanwise direction. This acts to spread the same amount of injectant over a larger volume if the time-averaged blowing ratio is the same with and without pulsations. The position of the shear layer described earlier also oscillates with respect to the wall in the pulsating flow.

The *first* region (mentioned earlier) at z/d from 0.0 to 0.46 contains the largest injectant concentrations, and the highest measured $-\overline{u'v'}$. As this shear layer oscillates to and from the wall at $z/d = 0.00$ and 0.23, the fluid containing the largest Reynolds stresses (i.e. the highest values of $-\overline{u'v'}$) also changes its vertical positions. Distributions are thus more spatially spread out which gives lower time-averaged magnitudes of maximum Reynolds shear stress $-2\overline{u'v'}/\overline{u}_\infty^2$ in Fig. 6. This figure also shows that the y/d locations of these *time-averaged* maxima in the pulsating flow do not change at $z/d = 0.00$ and 0.23 when compared to the flow with no pulsations.

At $z/d = 0.46$, Fig. 6 shows that the maximum

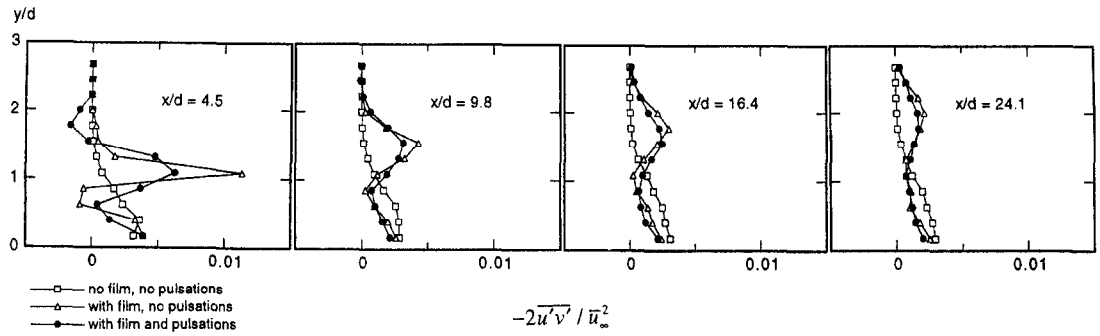

Fig. 7. Streamwise development of profiles of normalized $-2\overline{u'v'}$ Reynolds shear stress at $z/d = 0$ with quasi-steady film behavior.

$-2\overline{u'v'}/\overline{u_\infty^2}$ with pulsations is farther from the wall than the maximum value with no pulsations. Here, the maximum $-2\overline{u'v'}/\overline{u_\infty^2}$ with pulsations is also larger than the value in the film cooled boundary with no pulsations, perhaps because this location is near the edge of the most important injectant concentrations. Here, the vertical and spanwise oscillating motions of the injectant are speculated to agitate the nearby fluid thereby locally increasing $-\overline{u'v'}$.

In the *second* region at $z/d = 0.69$ and 0.91, Fig. 6 shows that the pulsations act to decrease $-2\overline{u'v'}/\overline{u_\infty^2}$ at $y/d > 1.1$, giving values which are more negative over small portions of the overall boundary layer thickness relative to the boundary layer with no pulsations.

The *third* region at $z/d = 1.14$ contains $-2\overline{u'v'}/\overline{u_\infty^2}$ profiles from the pulsating flow which approach baseline behavior (Fig. 6). Magnitudes of $-2\overline{u'v'}/\overline{u_\infty^2}$ match ones measured with film cooling and no pulsations and are lower than the ones measured in the baseline boundary layer (with no pulsations and no film) over the entire thickness of the layer.

Effects of pulsations on flow structure, variations with x/d

Figure 7 shows that magnitudes of $-2\overline{u'v'}/\overline{u_\infty^2}$ above and below the shear layer (near $y/d = 1.0$) change when pulsations are imposed. Values at $x/d = 4.5$ are more negative (above) at $y/d = 1.6$–2.3, and less negative (below) at $y/d = 0.4$–0.8 compared to the film cooled boundary layer with no pulsations. As x/d increases to 9.8–24.1, Fig. 7 shows that the $-2\overline{u'v'}/\overline{u_\infty^2}$ profiles measured with film cooling and pulsations approach the profiles measured with film cooling and no pulsations.

Overall effects of the pulsations

The changes in time-averaged structure evidence altered film behavior and altered turbulent transport from the pulsations. Consequently, the pulsations are also expected to produce alterations to time-averaged film effectiveness distributions.

EXPERIMENTAL RESULTS—FILM EFFECTIVENESS

Figure 8 shows variations of local adiabatic film effectiveness downstream of one injection hole across the span of the test surface. Results are given for film cooled turbulent boundary layers with no pulsations ($St_c = 0$), with quasi-steady pulsations ($St_c = 0.66$), and with non-quasi-steady-pulsations ($St_c = 8.85$). Although some small variations of η exist downstream of different injection holes, the ones in Fig. 8 for z/d from -1.5 to 1.5 are typical of the surveys made downstream of most of the holes. The results in Fig. 8, as well as in the following figure, were obtained at the same flow conditions as the injectant surveys presented in ref. [1]. Freestream velocity $\overline{u_\infty}$ is 2.0 m s^{-1}, $\overline{m} = 0.25$, and $\overline{u_\infty} d/\nu = 710$. Ridged trips placed just downstream of the injection hole inlets tripped the flow so that the injectant emerging from the holes is fully turbulent.

The most important differences between the three different pulsating flows occur at $x/d = 4.5$. Here, the quasi-steady η values ($St_c = 0.66$) are somewhat less than η values obtained with no pulsations ($St_c = 0$) over portions of the measurement span. Important decreases in local adiabatic film effectiveness then occur relative to no pulsation values when $St_c = 8.85$ and the pulsations are non-quasi-steady. With this situation, η are lower than values measured with no pulsations across most of the span of the measurement plane, particularly at and near $z/d = 0$. At x/d equal to 9.8 and 16.4, local η values from the boundary layers with quasi-steady and non-quasi-steady film behavior continue to be somewhat lower than $St_c = 0$ values near the same z/d locations. At $x/d = 24.1$, non-quasi-steady η values are significantly lower than ones measured in the boundary layers with no pulsations and with quasi-steady pulsations at all z/d from -1.5 to $+1.5$.

Centerline ($z/d = 0$) magnitudes of adiabatic film cooling effectiveness η_c are presented in Fig. 9 as they vary with x/d. The present results obtained with no pulsations ($St_c = 0$, $\overline{m} = 0.25$, $\rho_c/\rho_\infty \approx 0.90$) are in agreement with values from Pedersen *et al.* [9]

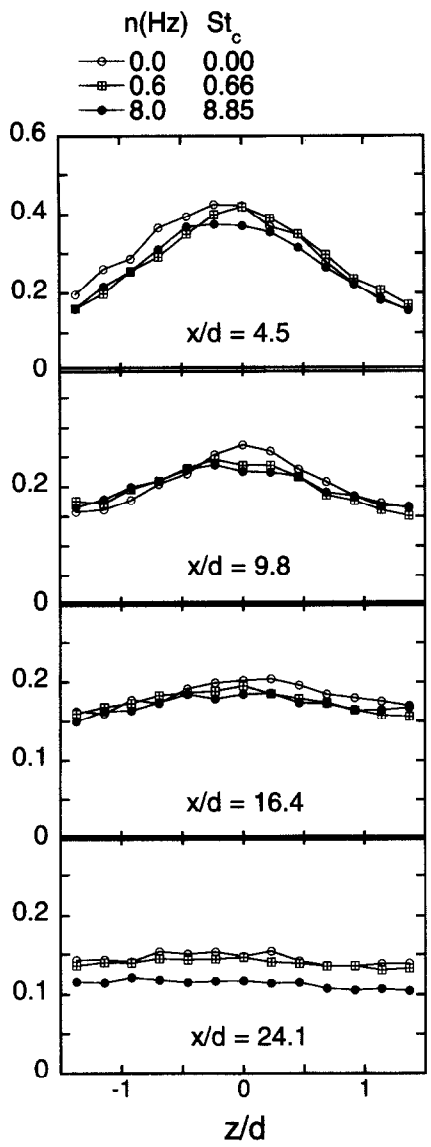

Fig. 8. Streamwise and spanwise variations of adiabatic film cooling effectiveness with no pulsations, quasi-steady film behavior, and non-quasi-steady film behavior, $\overline{m} = 0.25$.

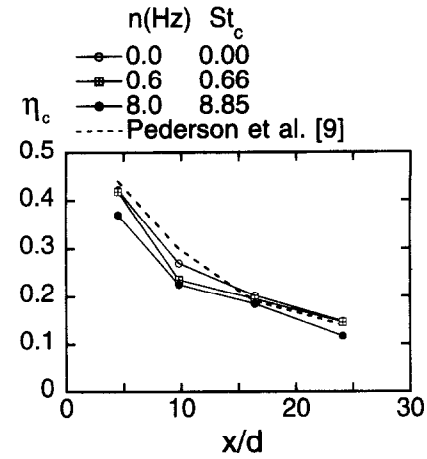

Fig. 9. Streamwise variation of centerline adiabatic film cooling effectiveness with no pulsations, quasi-steady film behavior, and non-quasi-steady film behavior, $\overline{m} = 0.25$.

measured at $\overline{m} = 0.213$ and $\rho_c/\rho_\infty = 0.954$, well within the uncertainty of the measurements. With both sets of results, both the boundary layer and injectant are turbulent, hole angles from the surface are 35°, and spanwise hole spacing is $3d$. The agreement between the $St_c = 0$ results and ones from ref. [9] is important because it validates the present experimental procedures.

Figure 9 shows the centerline film effectiveness with non-quasi-steady pulsations is reduced compared to values obtained with no pulsations for the entire range of x/d investigated. In particular, the non-quasi-steady η_c magnitude ($St_c = 8.85$) at $x/d = 4.5$ is reduced by 12% compared with the film cooled boundary layer with no pulsations ($St_c = 0$). Magnitudes of η_c measured with quasi-steady pulsations at $St_c = 0.66$ are close to values measured with no pulsations at all x/d measurement locations, with the exception of $x/d = 9.8$, where quasi-steady η_c are lower.

SUMMARY AND CONCLUSIONS

Experimental results are presented which describe the effects of bulk flow pulsations on turbulence structure and adiabatic film cooling effectiveness in a turbulent boundary layer film cooled using a single row of simple angle holes.

Important alterations to adiabatic film effectiveness result with non-quasi-steady pulsations at $St_c = 8.85$. In particular, reductions of local film effectiveness occur at x/d from 4.5 to 24.1 which are as large as 12% relative to the film cooled boundary layer with no pulsations. Effectiveness magnitudes measured with quasi-steady pulsations are either equivalent to or lower than values measured with no pulsations over the same x/d range. Different film effectiveness variations are thus observed with quasi-steady and non-quasi-steady film behavior. Because these two regimes of behavior are separated by coolant Strouhal numbers St_c equal to 1–2 [1], changes to film cooling protection are expected to occur over a wider range of film and boundary layer flow conditions than investigated here as St_c increases to become greater than 1–2.

Such changes occur because the film instantaneously changes its momentum and position in the boundary layer when bulk flow pulsations are imposed [1]. As a result, film concentrations move to and from the wall with each flow pulsation. When the injectant momentum at the injection hole exits is at its lowest during each pulsation cycle, the injectant is then located closer to the wall than the trajectory produced when no pulsations are imposed, and time-averaged streamwise velocities are locally lower than the velocities measured at $y/d < 1.0$–1.5 and x/d of 4.5, 9.8 and 16.4 when no pulsations are imposed. When the injectant momentum is at its highest during each pulsation cycle, the injectant is lifted farther away

from the wall than the trajectory produced with no pulsations, and time-averaged streamwise velocities are locally higher than the freestream velocity ($\bar{u}/\overline{u_\infty} > 1$) at $y/d = 1.5$–2.1 and x/d as large as 4.5. Consequently, the $\bar{u}/\overline{u_\infty}$ shear layer gradient produced by the film extends over a large vertical portion of the boundary layer at x/d of 4.5, 9.8 and 16.4 when the pulsations are imposed.

Important changes to profiles of time-averaged Reynolds shear stress $-2\overline{u'v'}$ are also present in the film cooled boundary layers because of the quasi-steady pulsations. These are particularly evident at $x/d = 4.5$ where the strong shear layer located in the outer portions of the largest film accumulations at $y/d = 0.9$–1.6 oscillates its positions with respect to the wall. As a result, the spatial extent of the shear layer increases, fluid with high stresses is more spread out spatially, and time-averaged magnitudes of maximum Reynolds shear stress $-2\overline{u'v'}/\overline{u_\infty^2}$ are lower. Many of the qualitative differences due to pulsations continue to be present as x/d increases to 9.8, 16.4 and 24.1. However, as the injectant becomes more diffuse, differences between the film cooled boundary layer with pulsations and the film cooled boundary layer with no pulsations generally tend to become less significant.

REFERENCES

1. P. M. Ligrani, R. Gong, J. M. Cuthrell and J. S. Lee, Bulk flow pulsations and film cooling—1. Injectant behavior, *Int. J. Heat Mass Transfer* **39,** 2271–2282 (1996).
2. A. E. Perry, *Hot-Wire Anemometry*. Clarendon Press, Oxford University (1982).
3. A. K. M. F. Hussain and W. C. Reynolds, The mechanics of an organized wave in turbulent shear flow, *J. Fluid Mech.* **41,** 241–258 (1970).
4. B. R. Ramaprian and S. W. Tu, An experimental study of oscillatory pipe flow at transitional Reynolds numbers, *J. Fluid Mech.* **100,** 513–544 (1980).
5. J. G. Green, Turbulence structure resulting from interactions between an embedded vortex and wall jet. M.Sc. thesis, Department of Mechanical Engineering, U.S. Naval Postgraduate School, Monterey, CA (1989).
6. P. S. Klebanoff, Characteristics of turbulence in a boundary layer with zero pressure gradient, NACA Technical Note 3178 (1954).
7. A. N. Menendez and B. R. Ramaprian, Experimental study of a periodic turbulent boundary layer in zero mean pressure gradient, *Aeronaut. J.* **93,** 195–206 (1989).
8. J. M Cuthrell, A study of film cooling and bulk flow pulsations. M.Sc. thesis, Department of Mechanical Engineering, University of Utah (1995).
9. D. R. Pedersen, E. R. G. Eckert and R. J. Goldstein, Film cooling with large density differences between the mainstream and the secondary fluid measured with the heat–mass transfer analogy, *ASME Trans. J. Heat Transfer* **99,** 620–627 (1977).